

Silicon quantum processor with robust long-distance qubit couplings

Guilherme Tosi,¹ Fahd A. Mohiyaddin,¹ Stefanie B. Tenberg,¹
Rajib Rahman,² Gerhard Klimeck,² and Andrea Morello¹

¹*Centre for Quantum Computation and Communication Technology,
School of Electrical Engineering & Telecommunications,
UNSW Australia, Sydney, New South Wales 2052, Australia.*

²*Network for Computational Nanotechnology, Purdue University, West Lafayette, Indiana 47907, United States
(Dated: October 26, 2021)*

Practical quantum computers require the construction of a large network of highly coherent qubits, interconnected in a design robust against errors. Donor spins in silicon provide a physical qubit platform compatible with the industry-standard semiconductor processing, together with state-of-the-art coherence and quantum gate fidelities. Here we present a scalable design for a silicon quantum processor that exploits the electric dipole induced on a donor by a top-gated metal-oxide-semiconductor structure. Quantum information can be encoded in either the nuclear spin or the flip-flop states of electron and nucleus. 1-qubit gates are obtained by low power electric and magnetic drive at microwave frequencies, while fast 2-qubit gates are mediated by the induced electric dipole. The scheme allows inter-qubit distances > 150 nm and is highly robust against donor placement uncertainties. Microwave resonators allow for millimeter-distance 2-qubit gates and interfacing with photonic links. The qubit states can be protected from charge noise up to second order, thus preserving the outstanding coherence times of spin qubits in silicon.

The successful implementation of quantum algorithms requires incorporation of error correction codes¹ that deal with the fragile nature of qubits. The highest tolerances in error rates are found when using nearest-neighbour topological codes², long-distance entanglement links^{3,4} or a combination of both⁵. There exist several physical platforms where state preservation^{6–8}, qubit control^{9–12} and 2-qubit logic gates^{9,13} are achieved with fault-tolerant fidelities. The ultimate goal is to integrate a large number of qubits in expandable arrays to construct a scalable, universal quantum processor.

Donor spin qubits in silicon are an appealing physical platform for that goal, due to the nanometric size of each unit, and the fabrication compatible with standard semiconductor processes¹⁴. By using isotopically enriched ²⁸Si as the substrate material¹⁵, donor spins offer coherence times approaching a minute⁸ and control error rates as small as 10^{-4} (ref. 12). However, integrating several of these qubits in a scalable architecture remains a formidable challenge, mainly because of the difficulty in achieving reliable 2-qubit gates.

The seminal Kane proposal¹⁶ for a nuclear-spin quantum computer in silicon described the use of short-range exchange interactions J between donor-bound electrons, to mediate an effective inter-nuclear coupling of order ~ 100 kHz. However, the exchange interaction has an oscillatory behaviour that can result in an of order magnitude variation in strength upon displacement by a single lattice site¹⁷. Notwithstanding, plenty of progress has been made in the experimental demonstration of the building blocks of a Kane-type processor^{18–21}, including the observation of inter-donor exchange^{22–24}. A series of recent proposals describes 2-qubit logic gates that are robust against large uncertainties in J (refs. 25 and 26), but still require extremely tight spacing between the qubits, typically $\sim 10 - 20$ nm. While few-qubit demon-

strations can certainly be built around tightly-spaced spins, large-scale architectures will require enough room to intersperse control gates and readout devices. Alternative proposals suggest the use of magnetic dipole interactions to mediate the gates^{27,28}, albeit at the cost of additional fabrication and operation complexity. The most established schemes for long-distance coupling between multiple qubits require the fabrication of long and precisely-placed chains of donors²⁹, posing formidable manufacturing hurdles.

Here we present a radical solution to all the challenges above. We describe a scalable donor-based quantum processor that does not require precise donor placement. The physical qubits are spaced by > 150 nm and coupled through direct electric dipole interactions and/or photonic links, while preserving their outstanding coherence times. This processor can be built using standard silicon Metal-Oxide-Semiconductor (MOS) processes for ultimate manufacturability.

Electrically-driven flip-flop qubit

The phosphorus donor in silicon comprises an electron spin $S = 1/2$ with gyromagnetic ratio $\gamma_e = 27.97$ GHz/T and basis states $|\downarrow\rangle, |\uparrow\rangle$, and a nuclear spin $I = 1/2$ with gyromagnetic ratio $\gamma_n = 17.23$ MHz/T and basis states $|\downarrow\rangle, |\uparrow\rangle$. The electron interacts with the nucleus through the hyperfine coupling A . When placed in a large magnetic field B_0 ($\gamma_+ B_0 \gg A$, with $\gamma_+ = \gamma_e + \gamma_n$), the eigenstates of the system are the separable tensor products of the basis states, i.e. $|\downarrow\uparrow\rangle, |\downarrow\downarrow\rangle, |\uparrow\downarrow\rangle, |\uparrow\uparrow\rangle$. The electron and the nucleus can be operated as independent single qubits by applying oscillating magnetic fields resonant with any of the transitions frequencies between eigenstates that differ by the flipping of one of the spins, e.g. $|\downarrow\uparrow\rangle \leftrightarrow |\uparrow\uparrow\rangle$ for the electron qubit, etc.

We envisage a device where a shallow ³¹P donor is em-

bedded in an isotopically pure ^{28}Si crystal at a depth z_d from the interface with a thin SiO_2 layer (Fig. 1a). The orbital wavefunction ψ of the donor-bound electron can be controlled by a vertical electric field E_z applied by a metal gate on top. It changes from a bulk-like donor state at low electric fields to an interface-like state at high-fields^{30,31} (insets in Fig. 1c). The hyperfine interaction $A(E_z)$, proportional to the square amplitude of the electron wavefunction at the donor site $|\psi(0, 0, z_d)|^2$, changes accordingly from the bulk value $A \approx 117$ MHz to $A \approx 0$ when the electron is fully displaced to the interface (Fig. 1c). At the “ionization point”, where the electron is shared halfway between donor and interface, $A(E_z)$ can vary strongly upon the application of a small voltage on the top gate. Shifting the electron wavefunction from the donor to the interface also results in the creation of an electric dipole $\mu_e = ed$, where e is the electron charge and d is the separation between the mean positions of the donor-bound and interface-bound wavefunctions ($d \lesssim z_d$, see Supplementary Information S1). The induced electric dipole μ_e has been largely overlooked in the past, but plays a crucial role in our proposal.

The key idea is to define a new qubit, called henceforth the *flip-flop qubit*, described in the subspace spanned by the states $|\downarrow\uparrow\rangle, |\uparrow\downarrow\rangle$. Since the basis states of the flip-flop qubit have the same (zero) total angular momentum, transitions between them cannot be driven by magnetic resonance. However, the eigenstates of the hyperfine interaction $A\mathbf{S} \cdot \mathbf{I}$ within the flip-flop qubit subspace are $(|\downarrow\uparrow\rangle - |\uparrow\downarrow\rangle)/\sqrt{2}, (|\downarrow\uparrow\rangle + |\uparrow\downarrow\rangle)/\sqrt{2}$ (Fig. 1b). Therefore, modulating $A(E_z)$ at the frequency

$$\epsilon_{\text{ff}}(A) = \sqrt{(\gamma_+ B_0)^2 + [A(E_z)]^2}, \quad (1)$$

corresponding to the flip-flop qubit energy splitting, causes an electric dipole transition between the $|\downarrow\uparrow\rangle, |\uparrow\downarrow\rangle$ basis states^{32,33}. A conceptually similar mechanism is involved in the resonant drive of a 3-electron, 2-dot hybrid qubit³⁴.

A quantum-mechanical description of the system is obtained by treating also the electron orbit as a two-level system (effectively a charge qubit; see Supplementary Information S1 for a justification of this two-level approximation), where the vertical position of the electron is represented by a Pauli σ_z operator, with eigenvectors $|d\rangle$, for the electron at the donor, and $|i\rangle$ at the interface (Fig. 1a,c). At the ionization point, in which the electron is equally shared between donor and interface, the energy difference between eigenstates $(|d\rangle - |i\rangle)/\sqrt{2}$ and $(|d\rangle + |i\rangle)/\sqrt{2}$ equals the tunnel coupling V_t between the donor and the interface potential wells. The simplified orbital Hamiltonian reads (in units of Hz):

$$\mathcal{H}_{\text{orb}} = \frac{V_t \sigma_x - [e(E_z - E_z^0)d/h] \sigma_z}{2}, \quad (2)$$

where E_z^0 is the vertical electric field at the ionization point, and h is the Planck constant. The electron ground

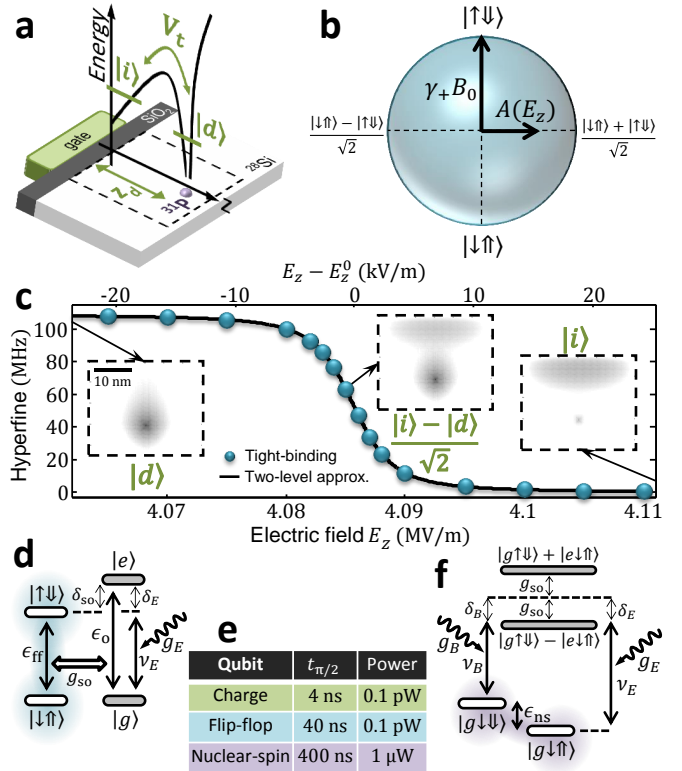


FIG. 1. Electric drive of Si:P spin qubits via hyperfine modulation. **a**, Qubit unit cell, in which the electron interface state, $|i\rangle$, is coupled to the donor-bound state, $|d\rangle$, by a tunnel rate V_t . Plot shows conduction band profile along z . **b**, Bloch sphere of a flip-flop spin qubit coupled to a vertical electric field E_z via the hyperfine interaction A . **c**, Atomistic tight-binding simulations³⁵ (dots) of the electron-nucleus hyperfine interaction, for a $z_d = 15.2$ nm deep donor, as a function of vertical electric field. The solid line is a fit using the simplified two-level Hamiltonian $\mathcal{H}_{\text{orb}} + \mathcal{H}_A^{\text{orb}}$, which yields $V_t = 9.3$ GHz (see Supplementary Information S1). Insets show the electron ground-state wavefunction, in the region within dashed lines in **a**, for three different vertical electric fields. **d**, Level diagram for electric-drive of flip-flop qubit. **e**, 1-qubit gate time for specified power, for each qubit. **f**, Level diagram for Raman-drive of nuclear-spin qubit, for $\delta_{\text{so}} = 0$.

$|g\rangle$ and excited $|e\rangle$ orbital eigenstates depend on $E_z - E_z^0$ (Fig. 1c) and have an energy difference given by:

$$\epsilon_o = \sqrt{(V_t)^2 + [e(E_z - E_z^0)d/h]^2} \quad (3)$$

Now we can write the hyperfine coupling as an operator that depends on the charge qubit state:

$$\mathcal{H}_A^{\text{orb}} = A \left(\frac{1 - \sigma_z}{2} \right) \mathbf{S} \cdot \mathbf{I}, \quad (4)$$

This results in a transverse coupling g_{so} between the flip-flop qubit and the electron orbit:

$$g_{\text{so}} = \frac{A V_t}{4 \epsilon_o} \quad (5)$$

A vertical electric field of amplitude E_{ac} , oscillating at a frequency ν_E equal to ϵ_o , would drive transitions between the charge eigenstates at a rate (half Rabi-frequency):

$$g_E = \frac{eE_{ac}dV_t}{4h\epsilon_o}. \quad (6)$$

To manipulate the flip-flop qubit states, it is preferable to introduce a detuning $\delta_{so} = \epsilon_o - \epsilon_{ff}$ between the charge and the flip-flop qubits, and drive E_{ac} at $\nu_E = \epsilon_{ff}$ (Fig. 1d). This results in a dispersive second-order coupling between flip-flop states and E_{ac} , at a rate:

$$g_E^{ff} = \frac{g_{so}g_E}{2} \left(\frac{1}{\delta_{so}} + \frac{1}{\delta_E} \right), \quad (7)$$

where $\delta_E = \epsilon_o - \nu_E$. If $\delta_E \gtrsim 10g_E$ and $\delta_{so} \gtrsim 10g_{so}$, the probability to occupy the charge excited state $|e\rangle$ is less than 1%³⁶, which minimizes the influence of charge decoherence while allowing sufficiently fast driving.

The fastest 1-qubit gates are obtained when the electron is at the ionization point, where $\partial A/\partial E_z$ is maximum, $\epsilon_o = V_t$, and both g_{so} and g_E are maximum (Eqs. 5 and 6). In particular, $g_{so} = A/4 = 29$ MHz, which requires at least $\delta_{so} = 290$ MHz to prevent orbital excitation. Since the AC drive happens is at resonance with the flip-flop qubit ($\nu_E = \epsilon_{ff}$), we need $\delta_E = \delta_{so}$. Choosing $g_E = \delta_E/10 = 29$ MHz and $d = 15$ nm requires an AC electric field $E_{ac} = 32$ V/m at the donor. In this case, the flip-flop qubit is driven at a Rabi frequency $2g_E^{ff} = 5.8$ MHz, yielding ~ 40 ns 1-qubit gates. This is achieved by applying an oscillating voltage on the top gate $V_{ac} \approx 3$ μ V, which corresponds to an incident power of only 0.1 pW. This is at least four orders of magnitude lower than the power needed to drive donor electron spin qubits, at the same Rabi frequency, with oscillating magnetic fields^{8,19}.

For a fixed value of B_0 and ϵ_{ff} , choosing δ_{so} requires the ability to tune the tunnel coupling V_t , which in turn depends on the donor depth below the Si/SiO₂ interface. In addition to the exponential dependence on depth, V_t also shows oscillations at the atomic scale³⁷, arising from a similar valley interference effect as that afflicting the exchange interaction¹⁷. In Supplementary Information S2, we show how V_t can be electrostatically tuned by using a gate stack identical to the well-established scheme for the confinement of single electrons in Si quantum dots¹¹. This allows to circumvent the effects of donor placement uncertainty inherent with ion implantation³⁸, while providing a dramatic reduction in the fabrication complexity, especially compared to schemes that require placing a gate *between* a pair of tightly-spaced donors¹⁶.

Raman drive of nuclear spin qubits

We now propose a novel method to coherently manipulate nuclear spin qubits, and controllably couple their

quantum states at large distances. The key idea is to combine the AC electric drive E_{ac} on the flip-flop qubit, with an additional AC magnetic field B_{ac} , perpendicular to the static B_0 . This results in a process analogous to a Raman transition³⁹, as shown in Fig. 1f: the AC electric and magnetic fields drive the nuclear-spin “up”, $|\downarrow\uparrow\rangle$, and “down”, $|\downarrow\downarrow\rangle$, states, respectively, to a virtual level close to the excited spin-charge states. As a result, the nuclear spin is driven via a second order process, without excitation of the electron spin or orbit.

The magnetic drive B_{ac} couples the electron spin states $|\downarrow\downarrow\rangle$ and $|\uparrow\downarrow\rangle$ at a rate:

$$g_B = \gamma_e B_{ac}/4 \quad (8)$$

The transition frequency between these states is $\epsilon_{ff} - \epsilon_{ns}$, where ϵ_{ns} is the nuclear spin transition frequency:

$$\epsilon_{ns}(A) = \frac{A(E_z)}{2} + \frac{\sqrt{(\gamma_+ B_0)^2 + [A(E_z)]^2} - \gamma_- B_0}{2}, \quad (9)$$

where $\gamma_- = \gamma_e - \gamma_n$. We choose the charge and flip-flop states to be in resonance, $\delta_{so} = 0$, since this yields best performance. The flip-flop and charge qubits give rise to hybridized eigenstates, $(|g\uparrow\downarrow\rangle - |e\downarrow\uparrow\rangle)/\sqrt{2}$ and $(|g\uparrow\downarrow\rangle + |e\downarrow\uparrow\rangle)/\sqrt{2}$, separated by $2g_{so}$ (Fig. 1f). If $|g_{so} + \delta_E| \gg g_E$, $|g_{so} - \delta_E| \gg g_E$, $|g_{so} + \delta_B| \gg g_B$ and $|g_{so} - \delta_B| \gg g_B$, excitation of these levels is prevented, while the nuclear spin is still Raman-driven via a second-order process at a rate:

$$g_E^{ns} = \frac{g_B g_E}{4} \left(\frac{1}{g_{so} + \delta_E} + \frac{1}{g_{so} - \delta_E} + \frac{1}{g_{so} + \delta_B} + \frac{1}{g_{so} - \delta_B} \right) \quad (10)$$

Fastest drive is achieved if $\delta_B = \delta_E = \delta_{so} = 0$, in which case $g_E^{ns} = g_B g_E / g_{so}$. For the earlier example of a ³¹P donor with $d = 15$ nm, choosing $g_B = g_E = g_{so}/10 = 2.9$ MHz ($E_{ac} = 3.2$ V/m and $B_{ac} = 0.4$ mT) yields a nuclear-spin Rabi drive frequency $2g_E^{ns} = 0.6$ MHz, corresponding to 0.4 μ s 1-qubit gates. This two orders of magnitude faster than the typical Rabi frequencies obtained with standard (NMR) magnetic drive at radiofrequency.

Cavity-mediated coupling of Si:P spin qubits

The use of electric dipole transitions allows a natural integration of donor-based spin qubits into a circuit-Quantum Electrodynamics (QED) architecture^{36,40}, by replacing the classical electric drive E_{ac} with the vacuum electric field of a microwave resonator, E_{vac} (Fig. 2a). A full quantum mechanical treatment yields the same coupling rates to photons as in Eqs. 6, 7 and 10. Therefore a vacuum field amplitude $E_{vac} = 32$ V/m can couple to a flip-flop qubit at a 2.9 MHz rate, three orders of magnitude faster than the electron-spin coupling rate to a resonator via its magnetic vacuum field⁴¹. This is comparable to the coupling strength obtained by using strong

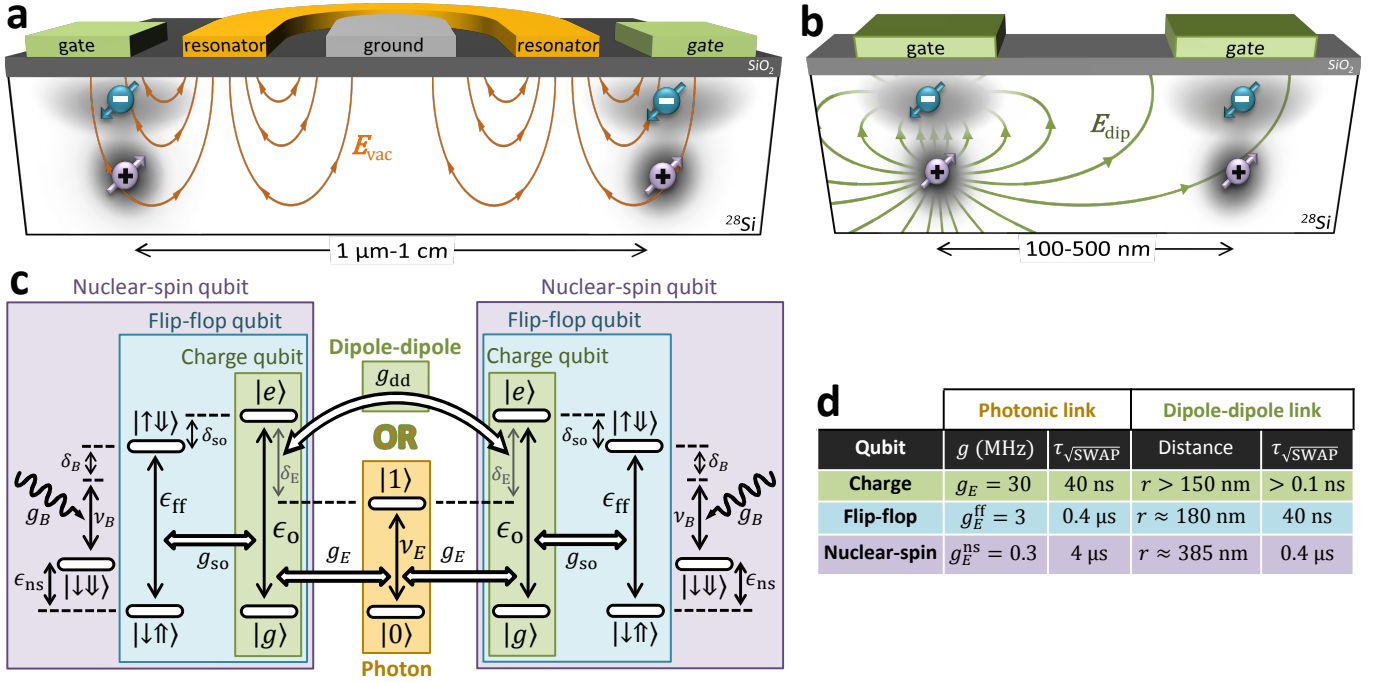


FIG. 2. **Coupling distant Si:P qubits.** **a**, Device scheme for coupling qubits via a photonic link. Distant donors, placed next to the resonator center line and biased to their ionization point, are subject vacuum electric field E_{vac} of a shared microwave resonator, resulting in effective 2-qubit couplings $(g_E^{\text{ff}})^2/\delta^{\text{ff}} \approx 0.3$ MHz and $(g_E^{\text{ns}})^2/\delta^{\text{ns}} \approx 30$ kHz. **b**, Device scheme for coupling qubits via electric dipole-dipole interaction, showing dipole field lines, E_{dip} , produced by the dipole on the left. **c**, Level diagram for distant two-qubit (charge, flip-flop and nuclear-spin) coupling via either virtual photons or direct dipole-dipole interaction. **d**, Optimal operation parameters for the three qubit types, through each distant coupling scheme.

magnetic field gradients^{42,43}, but without the need to integrate magnetic materials within a superconducting circuit. This value of vacuum field can be obtained by using planar transmission-line superconducting resonators operating at ≈ 10 GHz, where the gap between the center pin and the ground planes is shrunk to $\sim 10^{-7}$ m in the area where the donors are located.

As a further natural extension, single ^{31}P nuclear spins can be coupled to a microwave resonator by adding a classical AC magnetic drive. The qubit-photon coupling rate can reach 0.3 MHz if $E_{\text{vac}} = 3.2$ V/m. This is a striking observation, since the nuclear magnetic dipole is extremely small, and the spin normally only responds to resonant radio-frequencies excitation. This can be understood by noting that the nuclear spin is driven through the electric and magnetic dipole moments of the electron, and that it precesses at GHz frequencies in the AC magnetic drive rotating frame, $\epsilon_{\text{ns}} + \nu_B$.

The resonator can then be used as a quantum bus to couple two spin qubits separated by as far as 1 cm (Fig. 2a), a distance given by the mode wavelength. The detailed energy level diagrams to couple distant charge, flip-flop and nuclear spin qubits are shown inside green, aqua and purple rectangles, respectively, in Fig. 2c, with the linking resonator photon number state shown inside the orange rectangle. To avoid losses from photon decay, the qubits should be detuned from the resonator by an amount much greater than the qubit-photon coupling

rates. In the flip-flop case, this means $\delta_E^{\text{ff}} \gg g_E^{\text{ff}}$, where $\delta_E^{\text{ff}} = \nu_E - \epsilon_{\text{ff}}$. Two qubits are then coupled via a second-order process at a rate³⁶ $(g_E^{\text{ff}})^2/\delta^{\text{ff}}$. Assuming $\delta_E^{\text{ff}} = 10g_E^{\text{ff}}$, a 2-qubit $\sqrt{i\text{SWAP}}$ gate would take only 0.4 μs .

For the nuclear spins, the shared quantum electric field, E_{vac} , is sufficient to provide long-distance coupling, even though B_{ac} is a classical drive. This is analogous to proposals using trapped ions in optical cavities⁴⁴, charge qubits in microwave resonators⁴⁵ and silicon donors in photonic-crystal cavities⁴⁶. Photon creation is prevented if $\delta_E^{\text{ns}} \gg g_E^{\text{ns}}$, where $\delta_E^{\text{ns}} = \nu_E - (\epsilon_{\text{ns}} + \nu_B)$ is the qubit detuning from the resonator, in the magnetic drive rotating frame (Fig. 2c). Second-order perturbation theory shows that the 2-qubit coupling rate is $(g_E^{\text{ns}})^2/\delta_E^{\text{ns}}$. Again assuming $\delta_E^{\text{ns}} = 10g_E^{\text{ns}}$, this allows for $\sqrt{i\text{SWAP}}$ operations between distant ^{31}P nuclei to be performed within only 4 μs .

Two-qubit coupling via electric dipole interaction

We now present a new method to couple donor spins that lies at the heart of our scalable quantum processor. It exploits the electric dipole that naturally arises when a donor-electron wavefunction is biased to the ionization point (Fig. 2b), due to the fact that a negative charge has been partly displaced away from the positive ^{31}P nucleus. The electric field produced by this induced dipole can, in

turn, introduce a coupling term in a nearby donor which is also biased at the ionization point.

The interaction energy between two distant dipoles, μ_1 and μ_2 , oriented perpendicularly to their separation, r , is⁴⁷ $V_{\text{dip}} = \mu_1\mu_2/(4\pi\epsilon_r\epsilon_0r^3)$, where ϵ_0 is the vacuum permittivity and ϵ_r the material's dielectric constant ($\epsilon_r = 11.7$ in silicon). The electric dipole of each donor-interface state is $\mu_i = ed_i(1 + \sigma_{z,i})/2$, implying that the dipole-dipole interaction Hamiltonian is:

$$\mathcal{H}_{\text{dip}} = g_{\text{dd}} (\sigma_{z,1}\sigma_{z,2} + \sigma_{z,1} + \sigma_{z,2}) \quad (11a)$$

$$g_{\text{dd}} = \frac{e^2d_1d_2}{16\pi\epsilon_0\epsilon_r r^3\hbar} \quad (11b)$$

This electric dipole-dipole interaction is therefore equivalent to a transverse coupling term between the charge qubits (green rectangles in Fig. 2c) plus a small shift in the equilibrium orbital position of both electrons. Most importantly, since each flip-flop qubit is off-diagonally coupled to their electron position (Eq. 4), the electric dipole-dipole interaction provides a natural way to coupling two distant qubits.

Fig. 2c (inside aqua and green rectangles) shows the detailed level diagram to achieve that. For the flip-flop qubit, fastest coupling rates are achieved if all levels are in resonance, $\epsilon_{\text{ff}} = \epsilon_o$. If $\epsilon_o \gg g_{\text{dd}} \gg g_{\text{so}}$, electron orbital excitation is minimized and the flip-flop qubits are coupled at a rate, to second order:

$$g_{2q}^{\text{ff}} = (g_{\text{so}})^2/g_{\text{dd}} \quad (12)$$

For a pair of ³¹P donors with $d_1 = d_2 = 15$ nm, $g_{\text{dd}} \approx 10g_{\text{so}}$ requires $r = 180$ nm. At this distance, $g_{2q}^{\text{ff}} = 3$ MHz and therefore a $\sqrt{i\text{SWAP}}$ gate takes only 40 ns.

The electric dipole coupling strength has a linear dependence on donor dipole depth, and cubic on interdonor distance (Eq. 11b), making the electric-dipole mediated coupling of spins extremely robust against donor misplacement. Assuming ± 10 nm uncertainty, as expected from donor implantation³⁸, g_{dd} is predictable within an order of magnitude. This is in sharp contrast with coupling schemes based upon exchange interaction, where an order magnitude change in the value of J can arise from a displacement of even a single lattice site ($\ll 1$ nm)¹⁷.

Furthermore, nuclear spins can be coupled through the electric dipole term by adding an oscillating magnetic field with frequency close to the electron Zeeman frequency (purple rectangles in Fig. 2c).

At resonance, $\epsilon_o = \epsilon_{\text{ff}} = \nu_B + \epsilon_{\text{ns}}$. The electron spins are minimally excited if $g_B \ll (g_{\text{so}})^2/g_{\text{dd}}$, in which case the nuclear-spins are coupled at a rate, to second order:

$$g_{2q}^{\text{ns}} = \left(\frac{g_B}{g_{\text{so}}}\right)^2 g_{\text{dd}} \quad (13)$$

Fastest coupling is obtained if $g_{\text{so}} = g_{\text{dd}}$, which sets the optimal interdonor distance to $r = 385$ nm. Assuming $B_{\text{ac}} = 0.4$ mT ($g_B = g_{\text{so}}/10$), then $g_{2q}^{\text{ns}} = 0.3$ MHz. This yields a nuclear spin $\sqrt{i\text{SWAP}}$ gate time of 0.4 μs . This is a tremendous improvement over Kane's proposal¹⁶, for which a $\sqrt{i\text{SWAP}}$ gate between two ³¹P nuclear spins $r = 15$ nm apart takes 3 μs .

Charge noise insensitive operation

Since our operation and coupling scheme is based upon the use of charge qubits and electric dipoles, a natural concern is the fragility of the qubit states in the presence of charge or gate noise. Surprisingly, this turns out to be almost entirely avoidable, since the qubits can be operated at bias points that render either the flip-flop or the nuclear spin qubits highly insensitive from electrical noise.

At the ionization point, the energy splitting of the charge qubit is minimum and equal to V_t , and is therefore first-order insensitive to electric noise, $\partial\epsilon_o/\partial E_z = 0$ (Fig. 3a). Conversely, the bare flip-flop qubit energy is expected to depend strongly on E_z , through the combined effect of the hyperfine interaction A (Eq. 1, dotted curve in Fig. 3a), and the orbital dependence of the electron gyromagnetic ratio, γ_e . Indeed, the gyromagnetic ratio of an electron confined at a Si/SiO₂ interface can differ from that of a donor-bound electron by a relative amount Δ_γ up to 0.7% ⁴⁸. We therefore consider the electron Zeeman Hamiltonian to be dependent on the electron orbital position, i.e. the charge qubit σ_z operator:

$$\mathcal{H}_{B_0}^{\text{orb}} = \gamma_e B_0 \left[1 + \left(\frac{1 + \sigma_z}{2} \right) \Delta_\gamma \right] S_z - \gamma_n B_0 I_z, \quad (14)$$

where Δ_γ is the relative change in γ_e when the electron tunnels from the donor to the interface. We assume $\Delta_\gamma = -0.2\%$ ⁴⁸.

The overall flip-flop qubit transition frequency as a function of E_z becomes:

$$\epsilon_{\text{ff}}(A, \gamma_e) = \sqrt{[\gamma_e(E_z) + \gamma_n]^2 B_0^2 + [A(E_z)]^2}, \quad (15)$$

shown in Fig. 3a (dashed line), where we assumed $B_0 = 0.2$ T. $\epsilon_{\text{ff}}(A, \gamma_e)$ shows a steep slope around the ionization point, mostly caused by the E_z -dependence of γ_e (the dependence on A is less significant because A appears as a transverse term in flip-flop qubit basis). Therefore, while $E_z \approx E_z^0$ is the fastest operation point for 1- and 2-qubit gates driven by a resonant modulation of A , it is potentially the most prone to qubit dephasing from charge and gate noise, through the influence of E_z on γ_e .

However, computing instead the *full* flip-flop qubit Hamiltonian,

$$\mathcal{H}^{\text{ff}} = \mathcal{H}_{B_0}^{\text{orb}} + \mathcal{H}_A^{\text{orb}} + \mathcal{H}_{\text{orb}}, \quad (16)$$

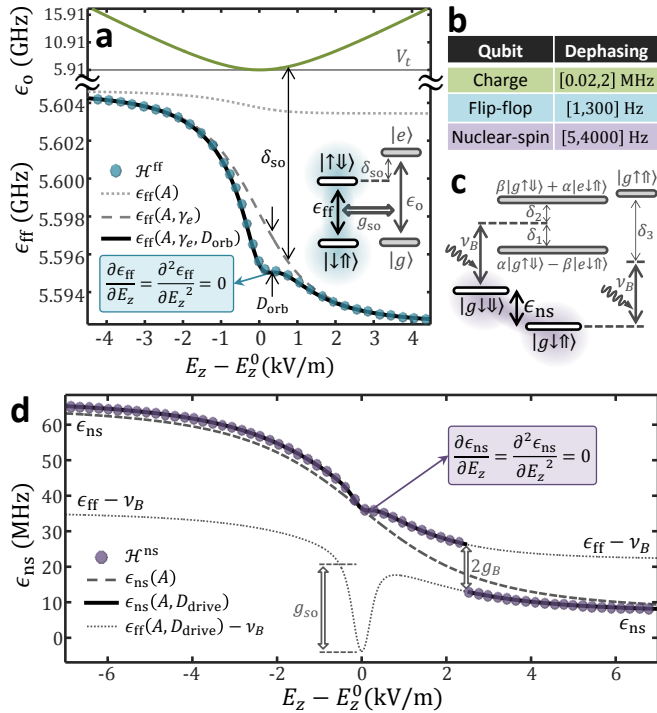


FIG. 3. **Second-order clock transitions.** **a**, Charge, ϵ_o , and flip-flop, ϵ_{ff} , qubits transition frequencies as a function of vertical electric field E_z , for $B_0 = 0.2$ T and $V_t = 5.91$ GHz. First and second derivatives of the flip-flop qubit frequency vanish at $E_z - E_z^0 = 330$ V/m. The inset shows the level diagram of flip-flop states coupled to electron-orbit states. **b**, Expected qubit dephasing rates assuming electric field fluctuations between $\Delta E_z^{\text{noise}} = [10, 100]$ V/m. **c**, Ladder of spin/orbit eigenstates relevant to the Raman drive of a nuclear spin. **d**, Nuclear spin transition frequency ϵ_{ns} as a function of vertical electric field E_z , for $B_0 = 0.4$ T, $V_t = \gamma_+ B_0$, $\nu_B = \gamma_e B_0 - A/4$ and $B_{\text{ac}} = 0.95$ mT. The nuclear spin transition frequencies (predominantly of the kind $|g \downarrow \uparrow\rangle \leftrightarrow |g \downarrow \downarrow\rangle$), calculated numerically from the full Hamiltonian, Eq. 19, are shown as purple dots and agree with Eq. 21a (thick line). The flip-flop transitions (predominantly $|g \downarrow \uparrow\rangle \leftrightarrow |g \uparrow \downarrow\rangle$), shown as dotted line, are shifted by g_{so} at $E_z = E_z^0$ through their resonant coupling to orbital levels, and also AC-Stark shifted by the magnetic drive through detunings δ_1 and δ_3 . The flip-flop transitions, in the rotating frame of the magnetic drive, ν_B , anticross with the nuclear-spin transitions at $E_z - E_z^0 = 2500$ V/m. First and second derivatives of the nuclear qubit frequency vanish at $E_z - E_z^0 = 200$ V/m.

reveals that the qubit transition frequency has an extra bend around the ionization point, due to the dispersive coupling to the electron orbit (inset in Fig. 3a). The resulting AC-Stark shift:

$$D_{\text{orb}}(E_z) = \frac{[g_{\text{so}}(E_z)]^2}{\delta_{\text{so}}(E_z)} \quad (17)$$

reduces the flip-flop qubit frequency to:

$$\epsilon_{\text{ff}}(A, \gamma_e, D_{\text{orb}}) = \epsilon_{\text{ff}}(A, \gamma_e) - D_{\text{orb}}(E_z), \quad (18)$$

The AC-Stark shift is largest around $E_z \approx E_z^0$, since

δ_{so} is lowest (i.e. the charge qubit frequency comes closest to the flip-flop qubit, Fig. 3a) and g_{so} is highest. Eq. 18 agrees with full numerical simulations of the Hamiltonian in Eq. 16 (Fig. 3a). Most importantly, it is possible to find conditions in which both the first and second derivatives of ϵ_{ff} with respect E_z vanish, and therefore the qubit transition frequency is highly immune from electric field noise. At this second-order ‘‘clock transition’’, Eq. 18 predicts that an electric field noise in the range $\Delta E_z^{\text{noise}} = [10, 100]$ V/m (a typical range for Si devices⁴⁹) shifts the qubit frequency by $\Delta \epsilon_{\text{ff}}^{\text{noise}} = [1, 300]$ Hz. An accurate calculation of the dephasing rate $1/T_2^*$ when ϵ_{ff} depends on noise only at the third order is beyond the scope of this work, but the above estimate already shows that the order of magnitude of $1/T_2^*$ might be comparable to the intrinsic electron spin dephasing in ²⁸Si, $1/T_2^* \approx 500$ Hz⁸, leading to the striking conclusion that the fast electrical operation and ability to couple qubits through their electric dipoles does not significantly impact their coherence. We note that the presence of a clock transition does not affect the ability to use E_{ac} to resonantly drive the qubit, since the transverse term in the Hamiltonian, $A(E_z)$, still responds fully to the electric field (this is similar to the case of magnetic clock transitions, e.g. in Si:Bi⁵⁰).

Similar considerations apply to the nuclear spin qubit driven through the Raman process. We discuss below the operation regime $\delta_B = \delta_{\text{so}} = 0$ since it yields the fastest qubit gates. The bare nuclear spin transition frequency depends roughly linearly on $A(E_z)$ (Eq. 9), which varies strongly with E_z around the ionization point (dashed line in Fig. 3d). However, when computed with the whole nuclear-spin Hamiltonian,

$$\mathcal{H}^{\text{ns}} = \mathcal{H}_{B_0}^{\text{orb}} + \mathcal{H}_A^{\text{orb}} + \mathcal{H}_{\text{orb}} + \mathcal{H}_{\text{ESR}}, \quad (19)$$

where \mathcal{H}_{ESR} is the magnetic drive Hamiltonian,

$$\mathcal{H}_{\text{ESR}} = B_{\text{ac}} \cos(2\pi\nu_B t)(\gamma_e S_z - \gamma_n I_z), \quad (20)$$

this nuclear transition frequency shows additional feature that arise from its coupling, via the magnetic drive, to higher-energy levels (see Fig. 3c for the definition of the levels and detunings). For $E_z \ll E_z^0$ (electron at the donor), $\epsilon_o \gg \epsilon_{\text{ff}}$ and therefore the flip-flop and charge eigenstates are decoupled ($\alpha = 1$ and $\beta = 0$ in Fig. 3c), and the magnetic drive is detuned ($\epsilon_{\text{ns}} + \nu_B \gg \epsilon_{\text{ff}}$). In these conditions, $\delta_1 > 0$ and $\delta_3 < 0$, therefore the levels $|g \downarrow \downarrow\rangle$ and $|g \uparrow \uparrow\rangle$ are AC-Stark shifted upwards and downwards, respectively. That explains why the nuclear spin transition frequency is slightly higher than the expected. As E_z approaches E_z^0 , ϵ_o becomes equal to ϵ_{ff} , and the flip-flop-orbit eigenstates become symmetric and anti-symmetric superpositions of the bare states ($\alpha = 1/\sqrt{2}$ and $\beta = 1/\sqrt{2}$ in Fig. 3c), separated by $2g_{\text{so}}$. At this ionization point δ_1 increases, decreasing the AC-Stark shift of the level $|g \downarrow \downarrow\rangle$. Also, δ_2 becomes small

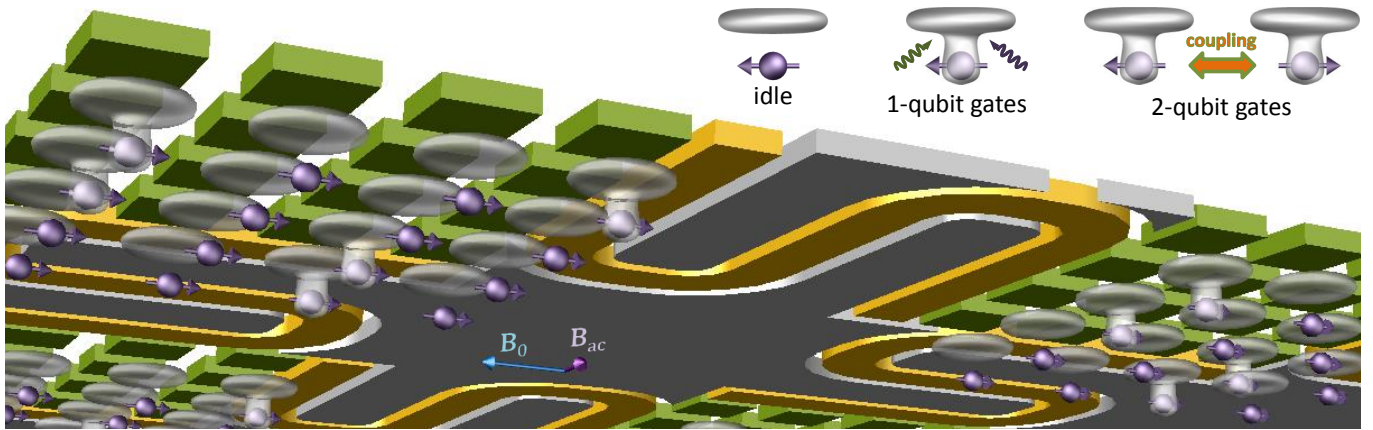


FIG. 4. **Silicon quantum processor.** Schematic view of a large-scale quantum processor based upon ^{31}P donors in Si, operated and coupled through the use of an induced electric dipole. We depict the case where quantum information is stored on the nuclear spin state of the donor. While the qubit is idle, the electron is pulled to the Si/SiO₂ interface by a voltage on the top gate (green), leaving the ^{31}P nucleus in the ultra-coherent ionized state. Single-qubit operations are achieved by adiabatically shifting part of the electron wavefunction towards the donor, and applying the Raman control sequences described in the text. The operation can be conducted while the qubit is at the 2nd-order clock transition. If two neighbouring donors are tuned at resonance (same $\epsilon_o, \epsilon_{\text{eff}}, \epsilon_{\text{ns}}$ in both), the electric dipole interaction mediates a 2-qubit \sqrt{i} SWAP entangling operation. The sketch shows a possible architecture where a cluster of qubits is locally coupled via the electric dipole, and a subgroup thereof is further coupled to another cluster through the interaction with a shared microwave cavity (orange). The same processor can be built around the flip-flop qubit instead of the ^{31}P nucleus, by operating the gates with E_{ac} only, and parking the electron fully at the donor during the idle phase. The drawing is not to scale; control lines, readout devices and microwave antennas are not shown.

enough as to AC-Stark-shift the $|g \downarrow \downarrow\rangle$ level to lower energies. These two effects of δ_1 and δ_2 produce the extra bend of the nuclear-spin transition frequency around $E_z = E_z^0$ (Fig. 3d). As E_z further increases, ϵ_o increases back again, and the flip-flop-orbit eigenstates return to the bare ones. Past this point, the magnetic drive gets in resonance with the electron spin transition ($\epsilon_{\text{ns}} + \nu_B = \epsilon_{\text{eff}}$), and the nuclear spin transition anticrosses with the flip-flop one. Finally, note that the flip-flop transition frequency, in the magnetic drive rotating frame, is lowered by its coupling rate to the electron orbit, g_{so} , at $E_z = E_z^0$.

We then model the qubit frequency by:

$$\epsilon_{\text{ns}}(A, D_{\text{drive}}) = \epsilon_{\text{ns}}(A) - D_{\text{drive}}(E_z), \quad (21a)$$

$$D_{\text{drive}}(E_z) = \sum_{i=1,2,3} \frac{\delta_i}{2} \left(\sqrt{1 + \left(\frac{2g_i}{\delta_i} \right)^2} - 1 \right), \quad (21b)$$

$$g_1 = \alpha g_B, \quad g_2 = \beta g_B, \quad g_3 = g_B \quad (21c)$$

This equation agrees with the full Hamiltonian simulations (Fig. 3d). Most importantly, there is a point close to the ionization point in which $\epsilon_{\text{ns}}(E_z)$ has both first and second derivatives equal to zero. Again assuming $\Delta E_z^{\text{noise}} = [10, 100]$ V/m, we find $\Delta \epsilon_{\text{ns}}^{\text{noise}} = [5, 4000]$ Hz. At the lowest limit, this is close to the dephasing rate of an ionized nuclear spin in ^{28}Si 8, leading again to the

striking conclusion that our scheme for operation and coupling through electric dipole transitions preserves the outstanding coherence of spin qubits in silicon.

Outlook: building a quantum processor

The control and coupling schemes for donor-based qubits described above provide a platform for the construction of a large-scale quantum processor, featuring several key advantages: (i) The gate operations are fast (Figs. 1e and 2d), despite requiring only very modest driving power; (ii) The large inter-qubit distances provide ample space for interconnects, and greatly relax the constraints on fabrication tolerances, including the precision of donor placement; (iii) Second-order ‘‘clock-transitions’’ preserve the outstanding coherence of spin qubits in ^{28}Si (Fig. 3b), despite the use of electric fields for control and coupling; (iv) All the relevant Hamiltonian parameters are widely tunable using simple gate layouts; (v) The possibility of coupling the qubits to microwave photons provides a path for photonic interconnects, as well as dispersive qubit readout; (vi) The fabrication of the processor is entirely compatible with standard silicon metal-oxide-semiconductor processing, and can be integrated with on-chip classical control circuitry. In Supplementary Information S3 we provide some guidelines for the practical implementation of these ideas. In Fig. 4 we draw a possible layout of a large-scale processor, incorporating cells of dipolarly-coupled qubits, interconnected by microwave photonic links. This scheme is known to yield very high fault-tolerance thresholds^{4,5}.

Our proposal constitutes a radical departure from existing schemes, and a plausible pathway to exploiting the

most coherent single qubit in the solid state - the ^{31}P nuclear spin of an ionised donor⁸ - in scalable architecture with robust, long-distance couplings.

-
- ¹ Terhal, B. M. Quantum error correction for quantum memories. *Rev. Mod. Phys.* **87**, 307 (2015).
- ² Fowler, A. G., Mariantoni, M., Martinis, J. M. & Cleland, A. N. Surface codes: Towards practical large-scale quantum computation. *Phys. Rev. A* **86**, 032324 (2012).
- ³ Knill, E. Quantum computing with realistically noisy devices. *Nature* **434**, 39–44 (2005).
- ⁴ Nickerson, N. H., Li, Y. & Benjamin, S. C. Topological quantum computing with a very noisy network and local error rates approaching one percent. *Nature Commun.* **4**, 1756 (2013).
- ⁵ Nickerson, N. H., Fitzsimons, J. F. & Benjamin, S. C. Freely scalable quantum technologies using cells of 5-to-50 qubits with very lossy and noisy photonic links. *Phys. Rev. X* **4**, 041041 (2014).
- ⁶ Maurer, P. C. *et al.* Room-temperature quantum bit memory exceeding one second. *Science* **336**, 1283–1286 (2012).
- ⁷ Saeedi, K., Simmons, S., Salvail, J. Z., Dluhy, P., Riemann, H., Abrosimov, N. V., Becker, P., Pohl, H.-J., Morton, J. J. L. & Thewalt, M. L. W. Room-temperature quantum bit storage exceeding 39 minutes using ionized donors in silicon-28. *Science* **342**, 830–833 (2013).
- ⁸ Muhonen, J. T. *et al.* Storing quantum information for 30 seconds in a nanoelectronic device. *Nature Nanotech.* **9**, 986–991 (2014).
- ⁹ Barends, R. *et al.* Superconducting quantum circuits at the surface code threshold for fault tolerance. *Nature* **508**, 500–503 (2014).
- ¹⁰ Harty, T. P., Allcock, D. T. C., Ballance, C. J., Guidoni, L., Janacek, H. A., Linke, N. M., Stacey, D. N. & Lucas, D. M. High-fidelity preparation, gates, memory, and readout of a trapped-ion quantum bit. *Phys. Rev. Lett.* **113**, 220501 (2014).
- ¹¹ Veldhorst, M. *et al.* An addressable quantum dot qubit with fault-tolerant control-fidelity. *Nature Nanotech.* **9**, 981–985 (2014).
- ¹² Muhonen, J. T. *et al.* Quantifying the quantum gate fidelity of single-atom spin qubits in silicon by randomized benchmarking. *Journal of Physics: Condensed Matter* **27**, 154205 (2015).
- ¹³ Benhelm, J., Kirchmair, G., Roos, C. F. & Blatt, R. Towards fault-tolerant quantum computing with trapped ions. *Nature Physics* **4**, 463–466 (2008).
- ¹⁴ Zwanenburg, F. A., Dzurak, A. S., Morello, A., Simmons, M. Y., Hollenberg, L. C., Klimeck, G., Rogge, S., Copper-Smith, S. N. & Eriksson, M. A. Silicon quantum electronics. *Rev. Mod. Phys.* **85**, 961 (2013).
- ¹⁵ Itoh, K. M. & Watanabe, H. Isotope engineering of silicon and diamond for quantum computing and sensing applications. *MRS Communications* **4**, 143–157 (2014).
- ¹⁶ Kane, B. E. A silicon-based nuclear spin quantum computer. *Nature* **393**, 133–137 (1998).
- ¹⁷ Koiller, B., Hu, X. & Das Sarma, S. Exchange in silicon-based quantum computer architecture. *Phys. Rev. Lett.* **88**, 027903 (2002).
- ¹⁸ Morello, A. *et al.* Single-shot readout of an electron spin in silicon. *Nature* **467**, 687–691 (2010).
- ¹⁹ Pla, J. J., Tan, K. Y., Dehollain, J. P., Lim, W. H., Morton, J. J. L., Jamieson, D. N., Dzurak, A. S. & Morello, A. A single-atom electron spin qubit in silicon. *Nature* **489**, 541–545 (2012).
- ²⁰ Pla, J. J., Tan, K. Y., Dehollain, J. P., Lim, W. H., Morton, J. J. L., Zwanenburg, F. A., Jamieson, D. N., Dzurak, A. S. & Morello, A. High-fidelity readout and control of a nuclear spin qubit in silicon. *Nature* **496**, 334–338 (2013).
- ²¹ Laucht, A. *et al.* Electrically controlling single-spin qubits in a continuous microwave field. *Science Adv.* **1**, e1500022 (2015).
- ²² Dehollain, J. P., Muhonen, J. T., Tan, K. Y., Saraiva, A., Jamieson, D. N., Dzurak, A. S. & Morello, A. Single-shot readout and relaxation of singlet and triplet states in exchange-coupled ^{31}P electron spins in silicon. *Phys. Rev. Lett.* **112**, 236801 (2014).
- ²³ Gonzalez-Zalba, M. F., Saraiva, A., Calderón, M. J., Heiss, D., Koiller, B. & Ferguson, A. J. An exchange-coupled donor molecule in silicon. *Nano letters* **14**, 5672–5676 (2014).
- ²⁴ Weber, B., Matthias, T. H., Mahapatra, S., Watson, T. F., Ryu, H., Rahman, R., L., H. C., Klimeck, G. & Simmons, M. Y. Spin blockade and exchange in coulomb-confined silicon double quantum dots. *Nature Nanotech.* **9**, 430–435 (2014).
- ²⁵ Kalra, R., Laucht, A., Hill, C. D. & Morello, A. Robust two-qubit gates for donors in silicon controlled by hyperfine interactions. *Phys. Rev. X* **4**, 021044 (2014).
- ²⁶ Pica, G., Lovett, B., Bhatt, R., Schenkel, T. & Lyon, S. Surface code architecture for donors and dots in silicon with imprecise and non-uniform qubit couplings. *arXiv:1506.04913* (2015).
- ²⁷ Trifunovic, L., Pedrocchi, F. L. & Loss, D. Long-distance entanglement of spin qubits via ferromagnet. *Phys. Rev. X* **3**, 041023 (2013).
- ²⁸ O’Gorman, J., Nickerson, N. H., Ross, P., Morton, J. J. & Benjamin, S. C. A silicon-based surface code quantum computer. *arXiv:1406.5149* (2014).
- ²⁹ Hollenberg, L. C. L., Greentree, A. D., Fowler, A. G. & Wellard, C. J. Two-dimensional architectures for donor-based quantum computing. *Phys. Rev. B* **74**, 045311 (2006).
- ³⁰ Calderón, M. J., Koiller, B., Hu, X. & Das Sarma, S. Quantum control of donor electrons at the Si-SiO₂ interface. *Phys. Rev. Lett.* **96**, 096802 (2006).
- ³¹ Lansbergen, G. P., Rahman, R., Wellard, C. J., Woo, I., Caro, J., Collaert, N., Biesemans, S., Klimeck, G., Hollenberg, L. C. L. & Rogge, S. Gate-induced quantum-confinement transition of a single dopant atom in a silicon finfet. *Nature Physics* **4**, 656–661 (2008).
- ³² Laird, E. A., Barthel, C., Rashba, E. I., Marcus, C. M., Hanson, M. P. & Gossard, A. C. Hyperfine-mediated gate-driven electron spin resonance. *Phys. Rev. Lett.* **99**, 246601 (2007).
- ³³ Luo, Y., Yu, H. & Yao, W. Deterministic preparation of

- Dicke states of donor nuclear spins in silicon by cooperative pumping. *Phys. Rev. B* **85**, 155304 (2012).
- ³⁴ Kim, D. *et al.* Microwave-driven coherent operation of a semiconductor quantum dot charge qubit. *Nature Nanotech.* **10**, 243–247 (2015).
- ³⁵ Klimeck, G. *et al.* Atomistic simulation of realistically sized nanodevices using NEMO 3-D – part i: Models and benchmarks. *IEEE Transactions on Electron Devices* **54**, 2079–2089 (2007).
- ³⁶ Blais, A., Huang, R.-S., Wallraff, A., Girvin, S. M. & Schoelkopf, R. J. Cavity quantum electrodynamics for superconducting electrical circuits: An architecture for quantum computation. *Phys. Rev. A* **69**, 062320 (2004).
- ³⁷ Calderón, M. J., Koiller, B. & Das Sarma, S. Model of valley interference effects on a donor electron close to a Si/SiO₂ interface. *Phys. Rev. B* **77**, 155302 (2008).
- ³⁸ van Donkelaar, J. *et al.* Single atom devices by ion implantation. *J. Phys.: Condens. Matter* **27**, 154204 (2015).
- ³⁹ Kok, P. & Lovett, B. *Introduction to Optical Quantum Information Processing* (Cambridge University Press, 2010).
- ⁴⁰ Xiang, Z.-L., Ashhab, S., You, J. Q. & Nori, F. Hybrid quantum circuits: Superconducting circuits interacting with other quantum systems. *Rev. Mod. Phys.* **85**, 623–653 (2013).
- ⁴¹ Tosi, G., Mohiyaddin, F. A., Huebl, H. & Morello, A. Circuit-quantum electrodynamics with direct magnetic coupling to single-atom spin qubits in isotopically enriched ²⁸Si. *AIP Advances* **4**, 087122 (2014).
- ⁴² Hu, X., Liu, Y.-x. & Nori, F. Strong coupling of a spin qubit to a superconducting stripline cavity. *Phys. Rev. B* **86**, 035314 (2012).
- ⁴³ Viennot, J. J., Dartailh, M. C., Cottet, A. & Kontos, T. Coherent coupling of a single spin to microwave cavity photons. *Science* **349**, 408–411 (2015).
- ⁴⁴ Pachos, J. & Walther, H. Quantum computation with trapped ions in an optical cavity. *Phys. Rev. Lett.* **89**, 187903 (2002).
- ⁴⁵ Feng, Z.-B. Coupling charge qubits via raman transitions in circuit qed. *Phys. Rev. A* **78**, 032325 (2008).
- ⁴⁶ Abanto, M., Davidovich, L., Koiller, B. & de Matos Filho, R. L. Quantum computation with doped silicon cavities. *Phys. Rev. B* **81**, 085325 (2010).
- ⁴⁷ Ravets, S., Labuhn, H., Barredo, D., Beguin, L., Lahaye, T. & Browaeys, A. Coherent dipole-dipole coupling between two single rydberg atoms at an electrically-tuned forster resonance. *Nature Phys.* **10**, 914–917 (2014).
- ⁴⁸ Rahman, R., Park, S. H., Boykin, T. B., Klimeck, G., Rogge, S. & Hollenberg, L. C. L. Gate-induced *g*-factor control and dimensional transition for donors in multivalley semiconductors. *Phys. Rev. B* **80**, 155301 (2009).
- ⁴⁹ Shi, Z. *et al.* Coherent quantum oscillations and echo measurements of a si charge qubit. *Phys. Rev. B* **88**, 075416 (2013).
- ⁵⁰ Wolfowicz, G., Tyryshkin, A. M., George, R. E., Riemann, H., Abrosimov, N. V., Becker, P., Pohl, H.-J., Thewalt, M. L. W., Lyon, S. A. & Morton, J. J. L. Atomic clock transitions in silicon-based spin qubits. *Nature Nanotech.* **8**, 561–564 (2013).

nication Technology (project number CE110001027), the US Army Research Office (W911NF-13-1-0024) and the Commonwealth Bank of Australia. Tight-biding simulations used NCN/nanohub.org computational resources funded by the US National Science Foundation under contract number EEC-1227110.

Correspondence should be addressed to G.T. (g.tosi@unsw.edu.au) or A.M. (a.morello@unsw.edu.au).

Acknowledgments We thank A. Blais, H. Bluhm, M. Eriksson and A. Laucht for discussions. This research was funded by the Australian Research Council Centre of Excellence for Quantum Computation and Commu-

SUPPLEMENTARY INFORMATION

S1. Validity of the two-level approximation for the electron orbital wavefunction

The concepts and calculations shown in the manuscript are based upon approximating the electron orbital degree of freedom as a two-level system, i.e. a charge qubit. The true orbital levels of a donor-interface system are, of course, more complex than that. However, below we show that the charge qubit model represents an excellent approximation, for the range of parameters relevant to our proposal.

The ground orbital wavefunction $|d\rangle$ of an electron bound to a donor is a symmetric combination of the 6 conduction band minima (“valleys”) ($k_{\pm x}$, $k_{\pm y}$, $k_{\pm z}$) in silicon^{S1}. Higher excited valley-orbit states are separated by > 10 meV and can be safely neglected. Conversely, the orbital states of an electron confined at the Si/SiO₂ interface comprise a low-energy doublet of states, with wavefunctions constructed as a combination of the $k_{\pm z}$ valleys. The k_{+z} and k_{-z} valleys are coupled by the abrupt potential of the interface, which breaks the degeneracy of the ground state doublet into the lower valley $|i\rangle$ and upper valley $|v\rangle$ states, separated by the valley splitting V_s ^{S2}. All the remaining excited donor and interface orbital states are well above the ground doublet by several meV^{S3,S4}. When the donor is close to ionization, the lowest-energy states of the system therefore consist of $|d\rangle$, $|i\rangle$ and $|v\rangle$ states, as shown in Fig. S1 inset.

We computed the above three energy levels with the atomistic tight binding package NEMO-3D^{S5,S6}, assuming a donor placed at depth $z_d = 15.2$ nm below the Si/SiO₂ interface, and biased close to the donor ionization field E_z^0 . The dependence of the energies of $|d\rangle$, $|i\rangle$ and $|v\rangle$ on electric field E_z is shown by the dots in Fig. S1. We also fit the lowest energy levels with the charge qubit two-level model described by the Hamiltonian \mathcal{H}_{orb} (in Eq. 2 of the main manuscript), and plot them as solid green lines in Fig. S1. The two-level model agrees well with tight-binding calculation taking $V_t = 9.3$ GHz and $d = 11$ nm in Eq. 2. Here, d represents the separation between the centre-of-mass positions of the donor-bound ($|d\rangle$) and interface-bound ($|i\rangle$) orbitals. This is the relevant quantity in calculating the electric dipole strength. The extracted value d is lower than the donor depth z_d , as expected, and is consistent with the separation between the mean positions of the donor and interface electron wavefunctions as modelled with NEMO-3D.

Fig. S1 shows that, when $E_z \ll E_z^0$, the orbital ground state $|g\rangle$ of the electron is localized at the donor, whereas the first excited state corresponds to the lower valley interface state. The two states are separated in energy by ϵ_0 , given by Eq. 3 of the main manuscript. As E_z increases, the two states approach, and anticross at $E_z = E_z^0$. For $E_z \gg E_z^0$, the donor state will eventually (at $E_z^v \sim 4.11$ MV/m) anticross with the upper valley interface state. Therefore, as shown by the solid

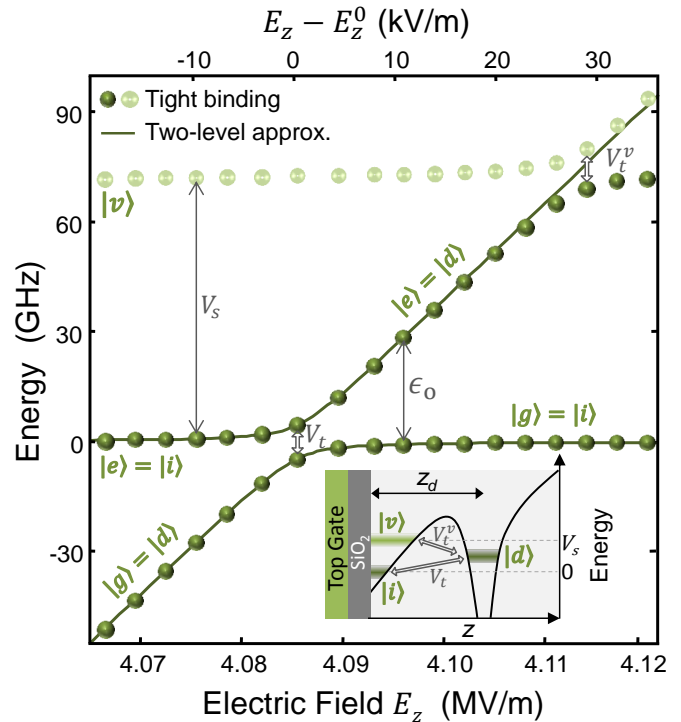


FIG. S1. The lowest orbital energy levels of the donor-interface system, with respect to the lower valley interface state $|i\rangle$ (set as the zero-energy reference). The donor is assumed 15.2 nm below a Si/SiO₂ interface. The dots correspond to the energy levels obtained from a full-scale tight-binding calculation with NEMO-3D. Solid lines represent the energy levels obtained from the two level approximation described by Eq. 2 in the main manuscript. An excellent agreement between our two level model and tight binding calculations is observed, since the valley splitting V_s is very much larger than the tunnel coupling V_t . Inset: Potential profile as a function of depth, illustrating the donor $|d\rangle$, lower $|i\rangle$ and upper $|v\rangle$ valley interface states. The donor ground state is tunnel coupled to the lower and upper valley interface states by V_t and V_t^v respectively.

lines in Fig. S1, a two-level model described by the $|d\rangle$ and $|i\rangle$ states constitutes an excellent approximation for $E_z < E_z^v$. This allows a broad range of validity of the simple charge qubit model, provided the interface valley splitting V_s is much larger than the tunnel coupling V_t . The NEMO-3D model used here predicts $V_s = 71.7$ GHz, which is indeed much larger than $V_t = 9.3$ GHz. Experimentally, even higher values of V_s are routinely observed in electrons confined at the Si/SiO₂ interface by top-gated structures^{S7}, providing further reassurance on the practical validity of our models.

S2. Tunnel coupling tunability between donor and interface

The tunnel coupling V_t of the electron between the donor and interface orbital states plays a key role in our

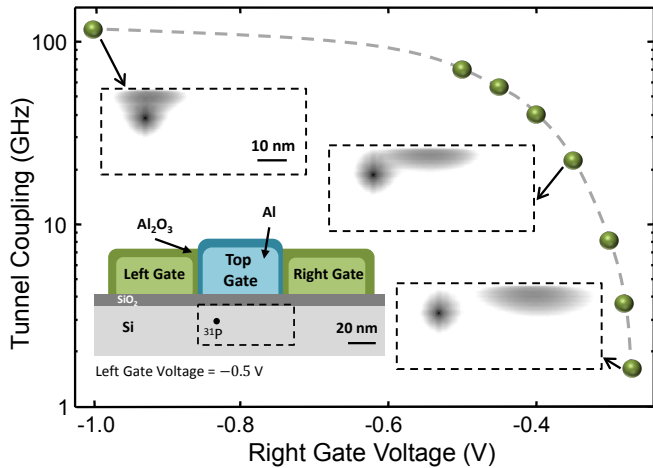


FIG. S2. Tunnel coupling V_t of electron as a function of gate voltage. To tune V_t , additional gates (left and right) are present on either side of the top gate which pulls the ^{31}P donor electron to the interface. The insets illustrate the NEMO-3D wavefunctions, when $V_r = -1, -0.35$ and -0.27 V. $V_l = -0.5$ V for all the simulations, and the top gate is biased such that the position of the electron is in between the donor and interface. The donor is assumed to be $z_d = 9$ nm below a SiO_2 interface.

models. It influences all the driving strengths (Eqs. 5,6,7 and 10) and inter-qubit couplings (Eqs. 12 and 13). In the presence of a single metal gate above the donor location, the dependence of V_t on donor depth has been analyzed with effective mass theory^{S4,S8}. Ref. S8 indicates that V_t depends exponentially with donor depth z_d , and decreases by an order of magnitude for every 6 nm increase in z_d . Moreover, due to the oscillatory nature of the donor and interface wavefunctions at the atomic scale, the tunnel coupling also has an oscillatory dependence on z_d , in addition to the exponential decay.

Using the ion implantation technique, the placement of a donor at $z_d \approx 15$ nm below the interface with a 5 nm thick oxide results in a vertical uncertainty of order ± 10 nm (Ref. S9), resulting in more than 2 orders of magnitude uncertainty in V_t . Therefore, it is crucial to implement a method to tune V_t *in situ*.

Here, we propose that V_t can be controlled by adding two gates (left and right) on either side of the gate (top) which pulls the donor electron to the interface. The relative voltages V_l and V_r applied to the left and right gates respectively can modify the potential landscape, and displace laterally the location of the interface wavefunction. This, in turn modifies the distance between the donor and interface wavefunctions allowing V_t to be significantly reduced. We use a combination of a finite element Poisson solver^{S10} and NEMO-3D to estimate V_t in this device topology. In Fig. S2 we plot the tunnel coupling tunability as a function of V_r , assuming $V_l = -0.5$ V and $z_d = 9.2$ nm. The insets of Fig. S2 show the NEMO-3D electron wavefunctions, when the top gate is biased such that the mean position of the electron is in between the

donor and interface. We infer that the electron wavefunction at the interface can be moved by several tens of nanometers with V_r , allowing V_t to be tuned by at least ~ 2 orders of magnitude. This technique therefore enables us to circumvent the uncertainty in donor depth and V_t arising from ion-implantation, while remaining straightforward from a nanofabrication point of view. Indeed, the gate layout used in this model is essentially identical to the layout routinely adopted for the fabrication of electrostatically-defined quantum dots at the Si/SiO₂ interface^{S7,S11}. These results indicate that a viable strategy for the construction of an ion-implanted quantum processor based upon our idea is to aim for an implantation depth that is by default rather shallow, then reduce V_t locally with the use of the surface gate stack.

S3. Operation of a quantum processor

On the basis of the physical mechanisms for controlling and coupling donor-based qubits described in the main text, a scalable quantum processor can be built using either the flip-flop or the nuclear spin as physical qubits, and the electric dipole-dipole interaction or the coupling to cavity photons for long-distance interactions between multiple qubits. There are numerous possible choices of architecture and error correction strategies that can be realized using our proposal. Below we give a brief description of some key considerations that could guide the design of a full quantum computer architecture.

The qubits should remain at noise-insensitive bias points, which can be three: electron at the donor; at the interface; or at the second order ‘‘clock transitions’’ near the ionization point. While the clock transition should be used for quantum gates, idle qubits are best decoupled from all other qubits by having the electron at the interface and the quantum state stored in the nuclear spin, which has record coherence times $T_2 \gtrsim 30$ s^{S12}. The switching between these states should be performed adiabatically, in order to allow keeping track of the (deterministic) phase shift accumulated by the qubit while moving from one resonance frequency to another. However, the switching period constitutes a time while the qubits are not protected against noise. Adiabaticity requires the switching time τ_s to be longer than $1/\epsilon_o$, but since $\epsilon_o \sim 10$ GHz, $\tau_s \sim 1$ ns would be adequate. This is a very short time window for noise to dephase the qubit.

1-qubit gates are performed through resonant drive, either with an AC electric field (flip-flop qubit), or a Raman process involving simultaneous electric and magnetic drive (nuclear spin). The duration and the phase of the driving pulse sets the axis and the rotation angle of the gate. In order to achieve high gate fidelities, it is important that the drive Rabi frequency is robust against electric noise. This is indeed satisfied for both the flip-flop and nuclear spin cases, since their Rabi frequencies, Eqs. 7 and 10, have a sweet spot around the ionization point. Ideally, these 1-qubit gates are performed while

the qubits are tuned to the clock-transitions. In this case, the gate times (Fig. 1e) are much shorter compared to the qubit dephasing times (Fig. 3b), and therefore extremely high fidelities are expected.

2-qubit gates are built from the effective exchange-like interactions that arise from the electric dipole coupling or the mediation of cavity photons. The interactions are gateable, since they are only effective while a pair of qubits is tuned in resonance, i.e. $\epsilon_o, \epsilon_{ff}$ (and ϵ_{ns} if using a nuclear spin) are the same at both sites, to within the strength of their relevant couplings. For the nuclear qubits, the electrons are brought towards their ionization points and at the second order clock transition, then an AC magnetic field B_{ac} is applied to both qubits to activate the electric dipole mediate coupling. The B_{ac} drive lasts for a time corresponding to \sqrt{i} SWAP operation, after which the electrons are quickly pulled to the interface and B_{ac} is turned off. For the flip-flop qubits, it suffices to tune both donors at the clock transition near the ionization point, for the time necessary to perform the desired \sqrt{i} SWAP operation. After operation, the electron should be moved fully to the donor, to prevent further spurious couplings to other qubits that might be tuned at the same resonance point.

Quantum information can be swapped between the nuclear and the flip-flop qubit by simply applying an ESR π -pulse that excites the $|\downarrow\downarrow\rangle$ state to $|\uparrow\downarrow\rangle$.

The qubit readout method depends on the chosen ar-

chitecture: in the presence of a resonant cavity coupled to the qubits, one can exploit the well-known dispersive, quantum non-demolition qubit readout allowed by the AC-Stark shift of the cavity frequency, conditional on the qubit state^{S13}. Near-quantum limited amplifiers have recently become available to obtain excellent readout speed and fidelities^{S14}. Without a cavity, the flip-flop qubit state can be read out in the same way as a bare electron spin, through spin-dependent tunnelling into a cold charge reservoir, combined with charge detection with e.g. a single-electron transistor^{S15}. The nuclear spin readout only requires an additional ESR pulse to map the nuclear state onto the electron spin, followed by electron readout^{S16}.

A large-scale, fault-tolerant architecture can be built in a variety of ways, depending upon the chosen coupling method. If using a resonant cavity, one can directly adapt the advanced schemes developed in the context of superconducting transmon qubits. With direct electric dipole couplings, 1- or 2-D arrays can be built to implement error correction schemes such as the Steane^{S17} or the surface^{S18} code, since all mutual qubit couplings are tunable and gateable. A more advanced processor can include a hybrid of both coupling methods, allowing nodes of nearest-neighbor coupled qubits to be interlinked through photons, in which case more advanced error-correction codes can be implemented^{S19-S22}.

-
- [S1] Kohn, W. & Luttinger, J. M. Theory of donor states in silicon. *Phys. Rev.* **98**, 915–922 (1955).
- [S2] Saraiva, A. L., Calderón, M. J., Hu, X., Das Sarma, S. & Koiller, B. Physical mechanisms of interface-mediated intervalley coupling in si. *Phys. Rev. B* **80**, 081305 (2009).
- [S3] Rahman, R. *et al.* Orbital stark effect and quantum confinement transition of donors in silicon. *Phys. Rev. B* **80**, 165314 (2009).
- [S4] Calderón, M. J., Saraiva, A., Koiller, B. & Das Sarma, S. Quantum control and manipulation of donor electrons in si-based quantum computing. *J. Appl. Phys.* **105**, 122410 (2009).
- [S5] Klimeck, G. *et al.* Atomistic simulation of realistically sized nanodevices using NEMO 3-D – part i: Models and benchmarks. *Electron Devices, IEEE Transactions on* **54**, 2079–2089 (2007).
- [S6] Klimeck, G. *et al.* Atomistic simulation of realistically sized nanodevices using NEMO 3-D – part ii: Applications. *Electron Devices, IEEE Transactions on* **54**, 2090–2099 (2007).
- [S7] Yang, C. H., Rossi, A., Ruskov, R., Lai, N. S., Mohiyaddin, F. A., Lee, S., Tahan, C., Klimeck, G., Morello, A. & Dzurak, A. S. Spin-valley lifetimes in a silicon quantum dot with tunable valley splitting. *Nature Commun.* **4** (2013).
- [S8] Calderón, M. J., Koiller, B. & Das Sarma, S. Model of valley interference effects on a donor electron close to a Si/SiO₂ interface. *Phys. Rev. B* **77**, 155302 (2008).
- [S9] van Donkelaar, J. *et al.* Single atom devices by ion implantation. *J. Phys.: Condens. Matter* **27**, 154204 (2015).
- [S10] <http://www.synopsys.com/TOOLS/TCAD/>.
- [S11] Veldhorst, M. *et al.* An addressable quantum dot qubit with fault-tolerant control-fidelity. *Nature Nanotech.* **9**, 981–985 (2014).
- [S12] Muhonen, J. T. *et al.* Storing quantum information for 30 seconds in a nanoelectronic device. *Nature Nanotech.* **9**, 986–991 (2014).
- [S13] Blais, A., Huang, R.-S., Wallraff, A., Girvin, S. M. & Schoelkopf, R. J. Cavity quantum electrodynamics for superconducting electrical circuits: An architecture for quantum computation. *Phys. Rev. A* **69**, 062320 (2004).
- [S14] Castellanos-Beltran, M., Irwin, K., Hilton, G., Vale, L. & Lehnert, K. Amplification and squeezing of quantum noise with a tunable josephson metamaterial. *Nature Phys.* **4**, 929–931 (2008).
- [S15] Morello, A. *et al.* Single-shot readout of an electron spin in silicon. *Nature* **467**, 687–691 (2010).
- [S16] Pla, J. J., Tan, K. Y., Dehollain, J. P., Lim, W. H., Morton, J. J. L., Zwanenburg, F. A., Jamieson, D. N., Dzurak, A. S. & Morello, A. High-fidelity readout and control of a nuclear spin qubit in silicon. *Nature* **496**, 334–338 (2013).
- [S17] Steane, A. Multiple-particle interference and quantum error correction. *Proceedings of the Royal Society of London A: Mathematical, Physical and Engineering*

- Sciences* **452**, 2551–2577 (1996).
- [S18] Fowler, A. G., Mariantoni, M., Martinis, J. M. & Cleland, A. N. Surface codes: Towards practical large-scale quantum computation. *Phys. Rev. A* **86**, 032324 (2012).
- [S19] Terhal, B. M. Quantum error correction for quantum memories. *Rev. Mod. Phys.* **87**, 307 (2015).
- [S20] Knill, E. Quantum computing with realistically noisy devices. *Nature* **434**, 39–44 (2005).
- [S21] Nickerson, N. H., Li, Y. & Benjamin, S. C. Topological quantum computing with a very noisy network and local error rates approaching one percent. *Nat. Commun.* **4**, 1756 (2013).
- [S22] Nickerson, N. H., Fitzsimons, J. F. & Benjamin, S. C. Freely scalable quantum technologies using cells of 5-to-50 qubits with very lossy and noisy photonic links. *Phys. Rev. X* **4**, 041041 (2014).